JOURNAL OF NEUROPHYSIOLOGY
Vol. 67, No. 2, February 1992. *Printed in U.S.A.*

Mathematical Model of an Identified Stomatogastric Ganglion Neuron

FRANK BUCHHOLTZ, JORGE GOLOWASCH, IRVING R. EPSTEIN, AND EVE MARDER
Departments of Chemistry and Biology, and Center for Complex Systems, Brandeis University, Waltham, Massachusetts 02254-9110

SUMMARY AND CONCLUSIONS

1. The ionic currents in the lateral pyloric (LP) cell of the stomatogastric ganglion (STG) described in the preceding paper of the rock crab *Cancer borealis* were fit with a set of differential equations that describe their voltage, time, and Ca^{2+} dependence. The voltage-dependent currents modeled are a delayed rectifier–like current, i_d; a Ca^{2+}-activated outward current, $i_{o(Ca)}$; a transient A-like current, i_A; a Ca^{2+} current, i_{Ca}; an inwardly rectifying current, i_h; and a fast tetrodotoxin (TTX)-sensitive Na^+ current, i_{Na}.

2. A single-compartment, isopotential model of the LP cell was constructed from the six voltage-dependent currents, a voltage-independent leak current i_l, a Ca^{2+} buffering system, and the membrane capacitance.

3. The behavior of the model LP neuron was compared with that of the biological neuron by simulating physiological experiments carried out in both voltage-clamp and current-clamp modes. The model and biological neurons show similar action-potential shapes, durations, steady-state current-voltage (*I-V*) curves, and respond to injected current in a comparable way.

INTRODUCTION

In the preceding paper (Golowasch and Marder 1992a) we described the ionic currents in the lateral pyloric (LP) cell of the stomatogastric ganglion (STG) of the rock crab, *Cancer borealis*. Specifically, we found that the LP neuron has at least three different voltage-dependent outward currents, and at least three important voltage-dependent inward currents. Additionally, we know that the LP neuron receives numerous synaptic inputs and is a direct target for neuromodulatory substances. In particular, the LP neuron is a direct target for the modulatory neuropeptide proctolin (Hooper and Marder 1987; Golowasch and Marder 1992b).

The LP neuron is an important component of the pyloric rhythm and routinely fires in bursts of action potentials, the timing of which is controlled by the inhibitory synaptic inputs to the LP as well as its intrinsic membrane properties. We eventually wish to explain how each of the membrane currents in a neuron that is part of a functional network contributes to its dynamical properties. In other words, we wish to understand, for each neuron in a network, how its activity within the network arises as a function of its voltage- and time-dependent currents and its synaptic and modulatory inputs.

Although biophysical data provide a great deal of information about individual membrane currents, the large number of currents expressed in most neurons makes it difficult to obtain a detailed understanding of how these currents interact when the neuron is not voltage clamped, but operating dynamically. Indeed, it is almost impossible to understand what each current contributes to the firing pattern of a neuron on the basis of experimental work alone for several reasons. First, we do not have pharmacological tools that allow the removal of each individual current completely without influencing other currents. Second, we are unable experimentally to increase the conductance of each current at will. Third, we have no good way of knowing, under current-clamp conditions, what each current is doing as the neuron fires.

Mathematical models of cells can provide a powerful tool with which to dissect and analyze the contributions of individual currents to the activity of the cell. Recent studies include a series of models of a thalamic neuron (Rose and Hindmarsh 1989a–c), a study showing the existence of chaos between the bursting and tonic firing modes of a model for the R15 cell in *Aplysia* (Canavier et al. 1990), a model exhibiting multiple modes of bursting activity in a conditionally bursting cell (Epstein and Marder 1990), and one of hippocampal CA3 cells (Traub et al. 1991).

In this paper we present a single-compartment model based on measurements of the ionic currents in the LP neuron (Golowasch and Marder 1992a). We compare the behavior of the model with the behavior of the biological LP neuron. In the following paper (Golowasch et al. 1992) we use this model to begin to understand the role of each of these currents in controlling the excitability of the LP neuron, and we examine the role of the proctolin-evoked inward current on neuronal excitability.

METHODS

The model consists of a set of differential equations of a form related to that developed by Hodgkin and Huxley (1952). In such a model, each ionic current is represented as the product of an activation a, a maximum conductance $\bar{g}$, and a driving force $(V - E_j)$. In some cases, there is an inactivation factor b as well

$$i_j = \bar{g}_j \cdot a^p \cdot b^q \cdot (V - E_j) \qquad (1)$$

where V is the membrane potential, E_j is the reversal potential of current i_j, a and b may take any values between 0 and 1, the exponent p may take integer values between 1 and 4, and the exponent q may take values 0 or 1.

The activation a of each current is described by a first-order differential equation of the form

$$da/dt = [a_\infty(V) - a] \cdot k_a(V) \qquad (2)$$

where $a_\infty(V)$ and $k_a(V)$ are the steady-state voltage dependence and relaxation rate, respectively, for the activation process.

The steady-state activation is voltage dependent and is of the form

$$a_\infty(V) = 1/\{1 + \exp[(V - V_a)/s_a]\} \quad (3)$$

where V_a is the half-maximal potential (i.e., the potential for which $a_\infty(V) = ½$), and s_a the step width of the curve (i.e., the range of potentials centered at V_a over which $a_\infty(V)$ varies from ~0 to ~1). We shall refer to *Eqs. 1–3* as our standard current, rate, and voltage-dependence equations, respectively. The inactivation variable b generally obeys the standard rate and voltage-dependence equations. Note that the "widths" s_a and s_b may be either positive or negative (Table 1). A negative s corresponds to a function that increases with V, that is to say, to an activation variable that increases with increasing depolarization. Positive s values generally describe inactivation variables (or the activation of the inwardly rectifying h current, see below).

The coupled nonlinear differential equations were integrated with an implicit backward Euler scheme (Press 1986). Initial conditions for each integration were calculated either by explicitly solving the steady-state equations or by integrating at the holding potential until all currents reached constant values. Parameters for individual currents were obtained from the measurements of the currents directly (Golowasch and Marder 1992a) or by integrating the model for the appropriate current under conditions that simulated the corresponding experiments and fitting the results. Because of the variability among cells (cf. Golowasch and Marder 1992a), fits were optimized by eye. Values for all parameters in our model are listed in Table 1. The exact Hodgkin-Huxley type equations could not be applied to the currents we have measured because, as mentioned in our previous paper (Golowasch and Marder 1992a), the forward and backward rate functions of the Hodgkin-Huxley method could not be measured directly (tail currents cannot be measured in the LP cell).

To simulate voltage-clamp experiments, we set dV/dt to zero, and fix the voltage V at the chosen holding potential V_h until steady-state conditions are achieved. Voltage pulses are then applied, and the required external current i_{ext} is calculated from *Eq. 4*. In simulations, a current is "blocked" by setting its maximum conductance $\bar{g}_j$ to zero, and a current is "isolated" by setting $\bar{g}_j$ of all other currents to zero.

RESULTS

Model

The model cell is isopotential. Therefore the membrane potential V is determined by

$$c_m \cdot dV/dt = i_{ext} - \sum_j i_j \quad (4)$$

where c_m is the capacitance of the membrane, i_{ext} is the externally applied current in current-clamp experiments, and $\sum_j i_j$ is the sum of the ionic currents described below.

Delayed rectifier, i_d

The main characteristic of this outward current is that it has an activation with a relatively long voltage-dependent delay, and no inactivation

$$i_d = \bar{g}_d \cdot n^4 \cdot (V - E_K) \quad (5)$$

The activation n and its voltage dependence n_∞ are given by our standard *Eqs. 2* and *3* (Fig. 1*B*). The relaxation rate $k_n(V)$ of the activation is voltage dependent

$$k_n(V) = c_n/\{1 + \exp[(V - V_{kn})/s_{kn}]\} \quad (6)$$

In Fig. 1*A* we compare the raw currents of an LP cell and the fit obtained with the use of *Eq. 5*. As can be seen, progressively stronger depolarizations lead to increasingly faster relaxations to the final state. This is better seen in the plot of the voltage dependence of the rate k_n (Fig. 1*B*). As in the Hodgkin-Huxley model of the squid axon (Hodgkin and Huxley 1952), an adequate fit to the initial lag of the activation process is obtained with an exponent of 4, and no inactivation is apparent.

Ca^{2+}-activated outward current, $i_{o(Ca)}$

Our experimental observations of $i_{o(Ca)}$ show that the current is rather complex, and these features are described

TABLE 1. *Parameters used in the model*

Conductance	Maximum Conductance $\bar{g}_j$, μS	Reversal Potential E_j, mV	Rate Constant, s^{-1}	Half-Maximum Potential, mV	Step Width, mV	Other Parameters
Delayed rectifier, i_d	$\bar{g}_d = 0.35$	$E_K = -80$	$c_n = 180$	$V_n = -25$ $V_{kn} = 10$	$s_n = -17$ $s_{kn} = -22$	
Calcium-activated outward current, $i_{o(Ca)}$	$\bar{g}_{o(Ca)} = 3.2$	$E_K = -80$	$k_{oa} = 600$ $k_{ob} = 35$ $k_{Ca} = 360$	$V_{ao1} = 0$ $V_{ao2} = -16$	$s_{ao1} = -23$ $s_{ao2} = -5$	$f = 0.6$ mV/μM $c_1 = 2.5$ μM $c_2 = 0.7$ μM $c_3 = 0.6$ μM [Ca°] = 0.05 μM $c_{iCa} = 300$ μM/nC
A-current, i_A	$\bar{g}_A = 2.2$	$E_K = -80$	$k_A = 140$ $k_{A1} = 50$ $c_{A2} = 3.6$	$V_A = -12$ $V_B = -62$ $V_{A2} = -40$ $V_X = 7$	$s_A = -26$ $s_B = 6$ $s_{A2} = -12$ $s_X = -15$	
Ca^{2+} current, i_{Ca}	$\bar{g}_{Ca1} = 0.21$ $\bar{g}_{Ca2} = 0.047$	E_{Ca}*	$k_{aCa1} = 50$ $k_{bCa1} = 16$ $k_{aCa2} = 10$	$V_{aCa1} = -11$ $V_{bCa1} = -50$ $V_{aCa2} = 22$	$s_{aCa1} = -7$ $s_{bCa1} = 8$ $s_{aCa2} = -7$	
Inward rectifier, i_h	$\bar{g}_h = 0.037$	$E_h = -10$	$c_r = 0.33$	$V_r = -70$ $V_{kr} = -110$	$s_r = 7$ $s_{kr} = -13$	
Fast Na^+ current, i_{Na}	$\bar{g}_{Na} = 2{,}300$	$E_{Na} = 50$	$k_m = 10{,}000$ $k_h = 500$	$V_{am} = -6$ $V_{bm} = -34$ $V_{ah} = -39$ $V_{bh} = -40$	$s_{am} = -20$ $s_{bm} = -13$ $s_{ah} = -8$ $s_{bh} = -5$	$c_{am} = 0.11$ mV^{-1} $c_{bm} = 15$ $c_{ah} = 0.08$
Leak current, i_l	$\bar{g}_l = 0.1$	$E_l = -50$				$c_m = 1.7$ nF

* $E_{Ca} = [R \cdot T/z \cdot F] \cdot \ln(13{,}000/[Ca^{2+}]_{in}) * 1{,}000$, and T was 283°K (10°C).

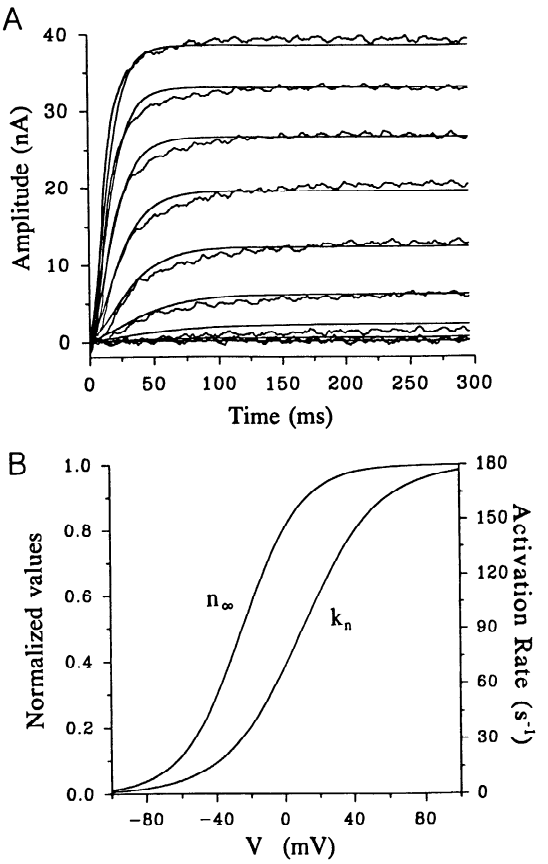

FIG. 1. Model i_d current. *A*: superimposed raw currents (noisy traces) described in Golowasch and Marder (1992a), and the model i_d current calculated from *Eq. 5*. $V_h = -40$ mV. At $t = 0$ ms, V_{test} pulses to $-50 \cdots +30$ mV in steps of 10 mV were applied. *B*: steady-state activation n_∞ and activation rate k_n plotted as a function of the membrane potential.

in Fig. 2. Following the literature (Barrett et al. 1982; Moczydlowski and Latorre 1983; Yamada et al. 1989), we incorporate the Ca^{2+} concentration ([Ca]) into the voltage dependence of the activation a_o. The current $i_{o(Ca)}$ is given by

$$i_{o(Ca)} = \bar{g}_{o(Ca)} \cdot a_o \cdot b_o \cdot (V - E_K) \quad (7)$$

The activation a_o depends on both V and [Ca], whereas the inactivation b_o is calcium, but not voltage dependent

$$da_o/dt = [a_{o\infty}(V, [Ca]) - a_o] \cdot k_{oa} \quad (8)$$

$$db_o/dt = [b_{o\infty}([Ca]) - b_o] \cdot k_{ob} \quad (9)$$

where the steady-state values are

$$a_{o\infty}(V, [Ca]) = 1/\{1 + \exp[(V - V_{ao1} + f \cdot [Ca])/s_{ao1}]\} \cdot 1/\{1 + \exp[(V - V_{ao2} + f \cdot [Ca])/s_{ao2}]\} \cdot [[Ca]/(c_1 + [Ca])] \quad (10)$$

$$b_{o\infty}([Ca]) = c_2/(c_3 + [Ca]) \quad (11)$$

Figure 2*B* shows the voltage dependence of the activation term $a_{o\infty}(V, [Ca])$ for different [Ca]. As can be seen, the basic properties described for other Ca^{2+}-activated K^+ currents are represented well by this equation, namely the increase in steepness (Barrett et al. 1982; Moczydlowski and Latorre 1983) as well as the shift of the curves along the voltage axis toward more hyperpolarized potentials (Barrett et al. 1982; Moczydlowski and Latorre, 1983; Yamada et al. 1989) as the [Ca] is increased. This current, however, contains a new feature, namely that the conductance reaches a maximum at a certain Ca^{2+} concentration (dependent on voltage, and in the μM range, Fig. 2*C*). This feature, which is not encountered in other Ca^{2+}-activated K^+ currents and is observed when exogenous Ca^{2+} is injected into the LP cell (Golowasch and Marder 1992a), was not explicitly built into our model of $i_{o(Ca)}$ but emerged unexpectedly in our fitting procedure. A comparison of the raw $i_{o(Ca)}$ and our calculated current is shown in Fig. 2*A*.

$$d[Ca]/dt = -c_{iCa} \cdot i_{Ca} - k_{Ca} \cdot [Ca] + k_{Ca} \cdot [Ca^\circ] \quad (12)$$

where i_{Ca} is the Ca^{2+} current described below and [Ca°] is the background intracellular [Ca], which we assume to be constant. The constant c_{iCa} relates the Ca^{2+} current to the volume of the cell according to

$$c_{iCa} = 1/(z \cdot F \cdot \text{Vol}) \quad (13)$$

where $z = +2$ is the valence of Ca^{2+}, F is the Faraday con-

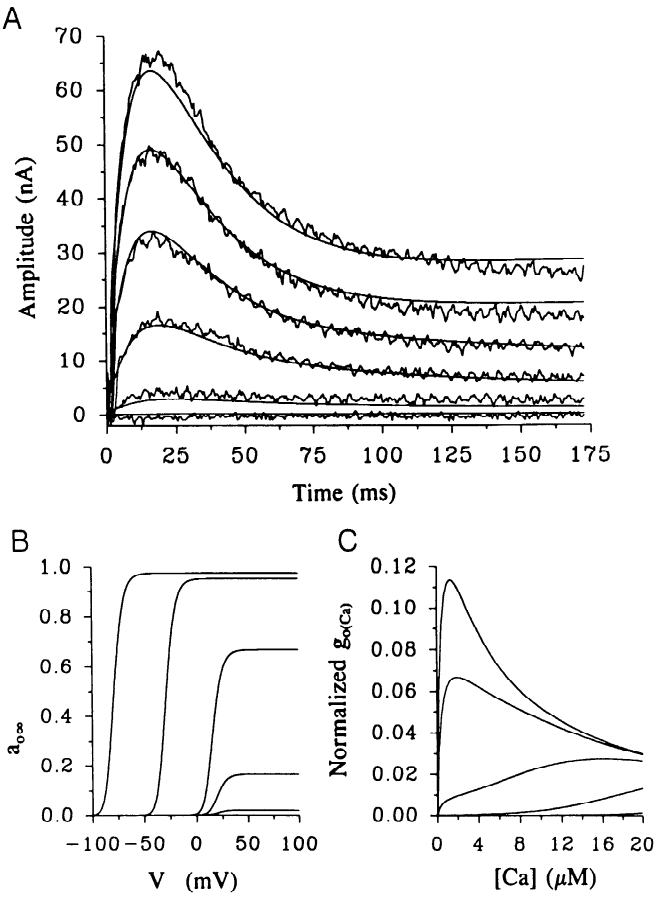

FIG. 2. Properties of the model Ca^{2+}-activated outward current. *A*: superimposed model current calculated from *Eqs. 7, 12*, and *17* and raw currents (noisy traces) measured in the LP cell as described in Golowasch and Marder (1992a). $V_h = -40$ mV. At $t =$ Oms, V pulses were applied to $-30 \cdots +20$ mV in increments of 10 mV. Notice that the underlying i_{Ca} and Ca^{2+} buffering system have been included in this fit. *B*: voltage dependence of the steady-state activation $a_{o\infty}$ (*Eq. 10*). Curves calculated with [Ca] set to 100, 50, 5, 0.5, and 0.05 μM (from *left* to *right*). *C*: normalized conductance vs. Ca^{2+} concentration at V values of +30, +20, +10, 0, and −10 mV (*top* to *bottom* traces). Notice that, at the more depolarized voltages, increasing [Ca] first increases $g_{o(Ca)}$ and then decreases it.

stant, and Vol is the volume in which the calcium dynamics occurs. If we use the volume of a typical 80-μm-diam LP cell body ($\sim 3 \times 10^{-7}$ ml) in *Eqs. 12* and *13*, we obtain a reasonable value to fit the measured slow kinetics of intracellular [Ca] changes that occur during the bursting of pyloric neurons (Graubard and Ross 1985; Ross and Graubard 1989), but this value for c_{iCa} is too small to fit the fast rise of the measured $i_{o(Ca)}$ in the LP cell (Fig. 2*A*) and the fast [Ca] changes observed in some STG cells with Ca^{2+}-imaging techniques (Graubard and Ross 1985; Ross and Graubard 1989). To get agreement with these measurements, we were forced to use a value of c_{iCa} about an order of magnitude higher. This implies that the effective volume in which Ca^{2+} is activating $i_{o(Ca)}$ is actually much smaller than the cell's volume and probably corresponds to the immediate vicinity of the inner cytoplasmic membrane (cf. Chad and Eckert 1984; Hernández-Cruz et al. 1990; Kramer and Zucker 1985; Traub et al. 1991; Zucker 1989). With these parameters, the kinetics of [Ca] due to spiking activity measured in pyloric neurons (Ross and Graubard 1989) agree reasonably well with those of intracellular [Ca] in the model cell [compare Fig. 5*a* of Ross and Graubard (1989) and *bottom panel* of Fig. 2 in Golowasch et al. (1992)].

Transient A-like current, i_A

The experimental data for i_A reveal that it is controlled by a voltage-dependent activation and two voltage-dependent inactivation processes. All three processes are described by our standard *Eqs. 2* and *3*. The relaxation rate $k_{A2}(V)$ for the second inactivation variable b_{A2} is voltage dependent

$$k_{A2}(V) = c_{A2}/\{1 + \exp[(V - V_{A2})/s_{A2}]\} \quad (14)$$

i_A is then given by

$$i_A = \bar{g}_A \cdot a_A{}^3 \cdot \{x(V) \cdot b_{A1} + [1 - x(V)] \cdot b_{A2}\} \cdot (V - E_K) \quad (15)$$

where $x(V)$ is a voltage-dependent weighting factor that determines the relative contributions of the two inactivation processes, favoring the slower b_{A2} term at lower voltages, and the faster b_{A1} term at more depolarized voltages

$$x(V) = 1/\{1 + \exp[(V - V_x)/s_x]\} \quad (16)$$

The superimposed measured and calculated i_A are shown in Fig. 3*A*. The model successfully reproduces the key features of this current, namely the voltage-dependent activation and the biphasic voltage-dependent inactivation processes. Figure 3*B* shows the activation, the inactivation, and the normalized conductance curves for the model i_A. The normalized conductance curve $i_A/[\bar{g}_A \cdot (V\text{-}E_K)]$ predicts that i_A should make a small contribution to the resting potential at around -50 mV. This issue is dealt with in the following paper (Golowasch et al. 1992).

Ca^{2+} current, i_{Ca}

The experimental observations indicate that i_{Ca} consists of two components, displaced from one another in voltage (Golowasch and Marder 1992a). One term involves both an activation and an inactivation process, whereas the other lacks inactivation. All processes, the two activations a_{Ca1} and a_{Ca2} and the inactivation b_{Ca1}, and their voltage dependences are described by our standard *Eqs. 2* and *3*. We take the three time-dependent variables to make up the single Ca^{2+} current, although we do not have experimental evidence to indicate whether the two conductance terms correspond to two independent conductances or not

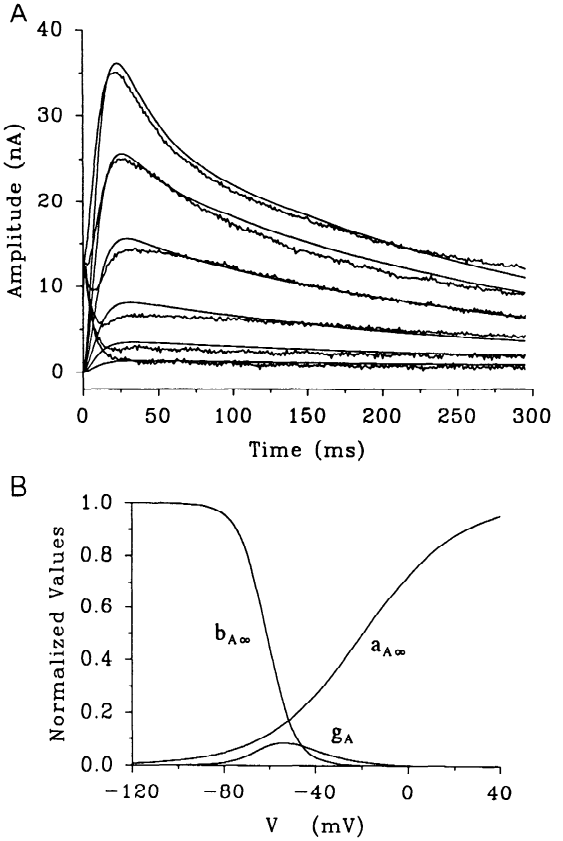

FIG. 3. Characteristics of the model i_A. *A*: superimposed current traces of i_A calculated from the model (*Eq. 15*) and the currents measured in the LP cell (noisy traces) as described in Golowasch and Marder (1992a). $V_h = -40$ mV. At t = Oms, V_{test} pulses were applied to $-40 \cdots +10$ mV in increments of 10 mV. *B*: voltage dependence of the steady-state activation $a_{A\infty}$, inactivation $b_{A\infty}$, and normalized conductance $g_A = i_A/[\bar{g}_A \cdot (V\text{-}E_K)] \cdot 100$ (factor of 100 used to amplify g_A for it to show at this scale).

$$i_{Ca} = (\bar{g}_{Ca1} \cdot a_{Ca1} \cdot b_{Ca1} + \bar{g}_{Ca2} \cdot a_{Ca2}) \cdot (V - E_{Ca}) \quad (17)$$

The Ca^{2+} equilibrium potential E_{Ca} is readjusted as the intracellular [Ca] changes because of Ca^{2+} influx (*Eq.* 12, Table 1).

Inwardly rectifying or hyperpolarization activated current, i_h

At voltages more hyperpolarized than the resting potential, V_{rest}, of the cell, a slow inward current is activated. The activity of this current appears to be determined by a single activation process. No inactivation has been observed. Thus a single set of equations (*Eqs. 2* and *3*) for the activation r and its voltage dependence $r_\infty(V)$, together with the voltage dependence of the relaxation rate $k_r(V)$, describe the time course of this inward current

$$k_r(V) = c_r \cdot \{1 + \exp[(V - V_{kr})/s_{kr}]\} \quad (18)$$

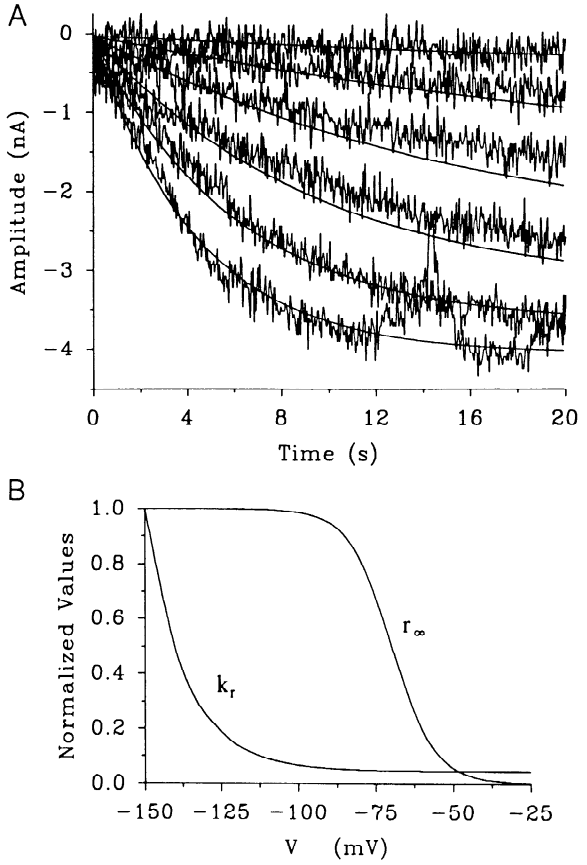

FIG. 4. Properties of i_h. *A*: current traces obtained from the LP cell as described in Golowasch and Marder (1992a) (noisy traces), and the model cell (*Eq. 19*). $V_h = -40$ mV. At $t = 0$ s, the voltage was stepped to $-120 \cdots -70$ mV in steps of 10 mV (*bottom* to *top*). *B*: normalized values of the steady-state activation r_∞ and the relaxation rate k_r (*Eq. 18*) as a function of the membrane potential.

The h current is given by

$$i_h = \bar{g}_h \cdot r \cdot (V - E_h) \tag{19}$$

Figure 4*A* shows the experimental data obtained by Golowasch and Marder (1992a) superimposed on the results of *Eq. 19*. The relaxation rate $k_r(V)$ becomes very small at voltages near V_{rest}, as can be seen from Fig. 4*B*, which shows the normalized $k_r(V)$ [i.e., $0.044 \cdot k_r(V)/c_r$] and the steady-state activation $r_\infty(V)$.

Fast Na$^+$ current, i_{Na}

Because it is likely that i_{Na} is generated far from the cell body, or even at the periphery of the central neuropil (Miller 1975; Raper 1979), accurately measuring i_{Na} in the LP neuron was not feasible. Therefore we have used a slightly modified version of the i_{Na} employed by Epstein and Marder (1990). The parameters were chosen to obtain firing of action potentials when the differential equations were integrated (*Eq. 4*). Although there are many combinations of parameters that support tonic firing in the absence of injected current, the requirement that the model cell fire action potentials over a range of injected current similar to that seen experimentally narrows considerably the acceptable range of parameters

$$i_{Na} = \bar{g}_{Na} \cdot m^3 \cdot h \cdot (V - E_{Na}) \tag{20}$$

The activation process m and the inactivation process h both obey *Eq. 2*. The voltage dependence of m is given by

$$m_\infty(V) = a_m(V)/[a_m(V) + b_m(V)] \tag{21}$$

with $a_m(V)$ and $b_m(V)$ given by

$$a_m(V) = c_{am} \cdot (V - V_{am})/\{1 - \exp[(V - V_{am})/s_{am}]\} \tag{22}$$

$$b_m(V) = c_{bm} \cdot \exp[(V - V_{bm})/s_{bm} \tag{23}$$

where k_m (and also k_h, see below) is in the usual Hodgkin-Huxley form $k_m = a_m(V) + b_m(V)$. Because this activation process is much faster than any of the other currents in this cell, we have also made the activation follow the voltage instantaneously (cf. Epstein and Marder 1990; Plant and Kim 1976) with essentially identical results.

The voltage dependence of h is

$$h_\infty(V) = a_h(V)/[a_h(V) + b_h(V)] \tag{24}$$

with $a_h(V)$ and $b_h(V)$ given by

$$a_h(V) = c_{ah} \cdot \exp[(V - V_{ah})/s_{ah}] \tag{25}$$

$$b_h(V) = 1/\{1 + \exp[(V - V_{bh})/s_{bh}]\} \tag{26}$$

and the rate constant $k_h = a_h(V_m) + b_h(V_m)$.

Leak current, i_l

The leak current consists simply of the linear component of the steady-state current-voltage (I-V) curve. It can be described by

$$i_l = \bar{g}_l \cdot (V - E_l) \tag{27}$$

The value of $\bar{g}_l$ was obtained by measuring the input conductance of LP neurons in the region of their I-V curve with lowest conductance (between -40 and -60 mV). Similar values were obtained when some of the voltage-dependent currents were pharmacologically blocked. The reversal potential of i_l is extremely close to the resting potential of the isolated cell with i_{Na} blocked, as could be determined by pharmacologically eliminating (Golowasch 1990) the ionic currents the LP cell expresses.

Capacitance

Unlike most of the other parameters, the value selected for c_m was influenced in large measure by the results of the whole-cell simulations. The membrane capacitance was one of the most critical parameters to be adjusted for the model cell to perform correctly. The value we finally chose, 1.7 nF, corresponds to ~8.5 times the somatic capacitance of the LP cell (assuming a radius of 80 μm and a specific capacitance of 1 μF/cm^2) and ~10 times lower than the total measured c_m of the LP cell (Golowasch and Marder 1992a). This low value leads us to make the assumption that the model represents a region equivalent to the action-potential spike generation zone. Values that differ by ≥20% from this cause the activity of the model cell to show dramatic alterations. Higher values produce damped oscillations of the membrane potential to a depolarized steady state. Lower values show relatively well-behaved tonic firing of action potentials, but the model does not respond properly to injected current.

Constructing the model

After modeling each of the currents as detailed above, we combined the individual currents according to *Eq. 4*. To test the model, we simulated current-clamp and voltage-clamp experiments in which we perturbed the model as a physiologist might perturb the biological neuron, and the behavior of the model was compared with the behavior of the biological LP neuron. Figure 5 shows a comparison of the unperturbed activity of the biological LP neuron (Fig. 5*A*) and the model LP neuron (Fig. 5*B*). Note that both the model and real cells fire action potentials spontaneously from a baseline potential of −45 to −50 mV. The frequency of spontaneous activity is similar. One notable difference is that the action potentials in the biological LP neuron are smaller in amplitude, as they are generated at a distance from the somatic recording site (Miller 1975; Raper 1979). Note also that the model's action potentials are slightly longer in duration than those of the real neuron in this example.

Figure 6*A* shows a comparison of the steady-state *I-V* curves of the experimental and the model LP cells with i_{Na} blocked (in TTX and $\bar{g}_{Na} = 0$, respectively). These curves were obtained in voltage clamp (real neuron) at near steady-state conditions (at the end of 1-s pulses), and in true steady-state conditions in simulated voltage clamp (model cell). Figure 6*B* shows superimposed plots of the *I-V* curves of the individual currents of the model LP neuron. These curves show that the model cell reproduces the steady-state properties of the LP cell rather well (see Golowasch and Marder 1992a). Note that as would be expected from the recordings in Fig. 5, the zero current intercept is −45 to −50 mV in both cases (Fig. 6*A*). Also evident is the finding that the input resistances are quite close to each other, and that the conductance of both neurons increases sharply as the cell is depolarized past −30 mV. The only discrepancy between the two cells is seen in the slight inflection shown by the model neuron at around −90 mV.

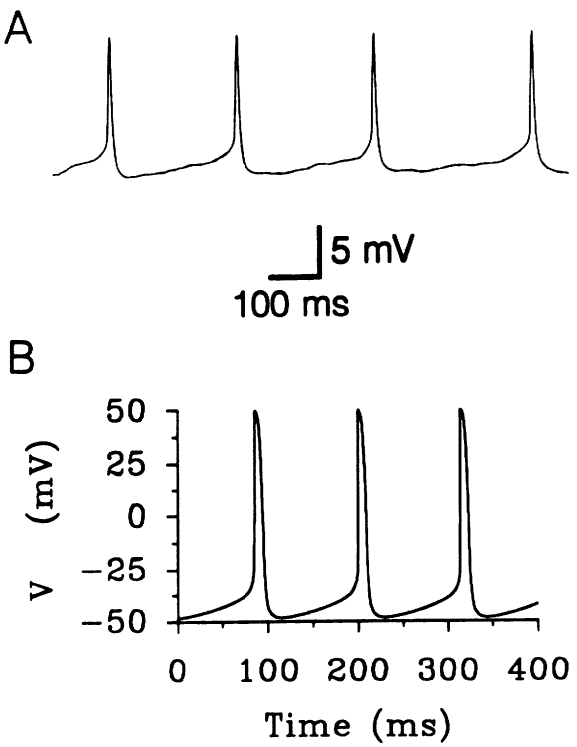

FIG. 5. Comparison of the activity patterns of the biological and the model LP neurons. *A*: intracellular recording from an LP neuron isolated from other inputs by placing it in 10^{-5} M picrotoxin (PTX) and by blocking impulse traffic in the stomatogastric nerve. Baseline membrane potential is approximately −45 mV. *B*: output of the model neuron with no external current imposed.

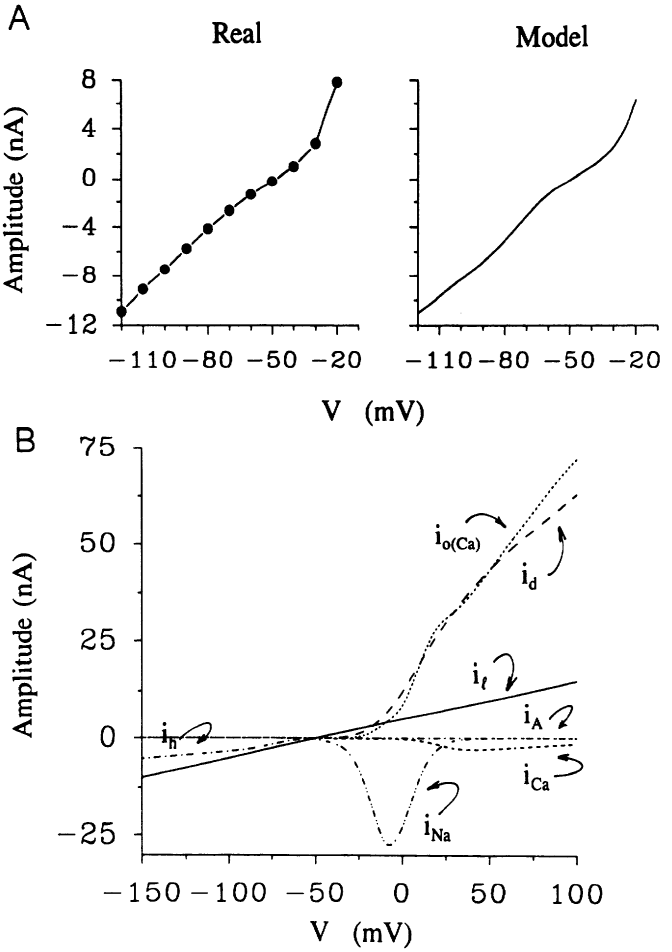

FIG. 6. Steady-state *I-V* curves. *A*: *I-V* curves of the experimental (*left*) and the model (*right*) cells. The experimental measurement was made at the end of a pulse of 1 s in control saline containing TTX and PTX. For the model cell the curve corresponds to the sum of the steady-state values of all the currents. In both cases i_{Na} is removed (experimentally with TTX, and by setting $\bar{g}_{Na} = 0$ in the model). *B*: steady-state *I-V* relationships of individual currents of the model cell, as given by *Eqs. 5, 7, 15, 17, 19, 20*, and *27*. i_A is not resolved at this scale and shows as a straight line through 0 nA.

Most of the currents show relatively simple steady-state *I-V* curves (Fig. 6*B*), as expected from the form of their activation and inactivation variables, *Eqs. 2* and *3*.

As shown by the blocking effect of TTX on the action potentials, i_{Na} is the current underlying action-potential generation. Its contribution to the steady-state *I-V* curve of the model cell (Fig. 6*B*) suggests that it only contributes minimally to the V_{rest} of the LP cell. Indeed, experiments indicate that this contribution is probably quite negligible, because bath application of TTX to a pharmacologically completely isolated LP cell (i.e., in PTX and the stomatogastric nerve blocked) has little effect on V_{rest}. Alternatively, this lack of any effect could be due to a shunting of the already

small i_{Na} by the membrane along the path between the spike initiation zone and the cell body, so that, as seen in the soma where the recordings are made from, TTX effectively fails to block any detectable current.

An important test of the model cell is the effect of current injection (Fig. 7). Positive current injection into the real LP cell causes the cell to depolarize and fire action potentials at a frequency that depends on the amount of current injected. With +5 nA, for example, it depolarizes by ~30 mV and fires at ~40 Hz (Golowasch 1990). With the same current injection, the model cell depolarizes by ~20 mV and fires at ~40 Hz (Fig. 7). When negative current is injected, the cells hyperpolarize and stop firing action potentials (Golowasch 1990). In the model cell, negative current injection also suppresses action potentials and produces a hyperpolarization that reflects an input resistance of the cell of ~10 MΩ. A strong enough negative current injection activates the development of a depolarizing voltage sag that reflects the activation of i_h (*bottom trace*, Fig. 7) (see also Golowasch 1990).

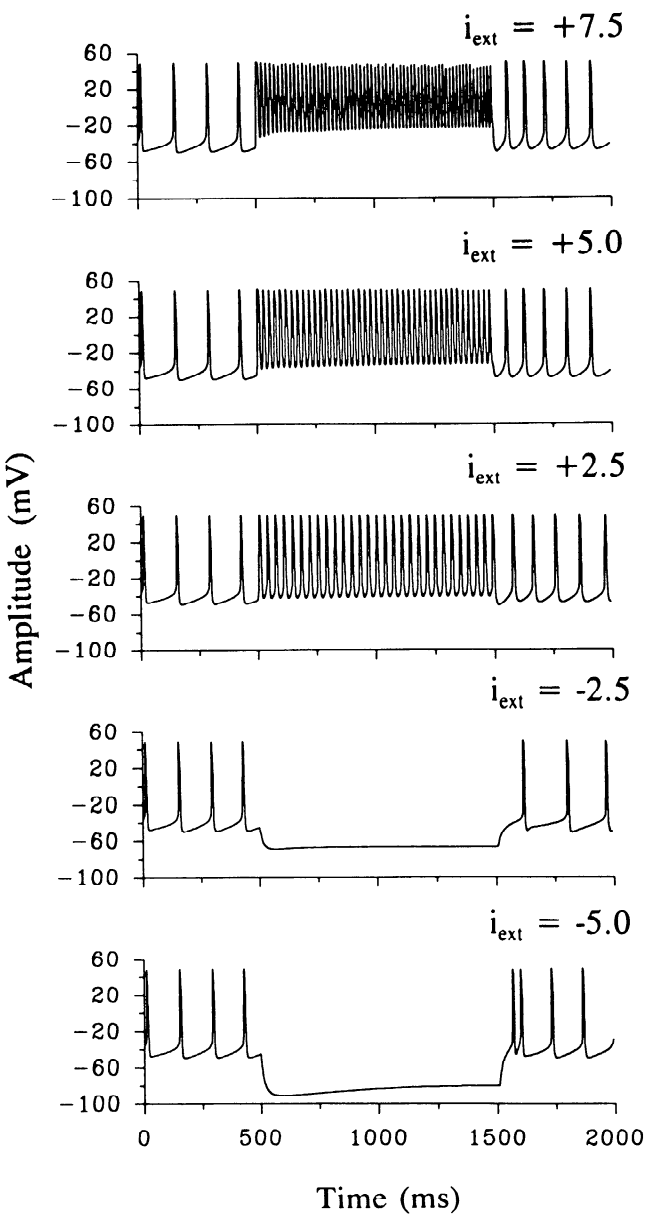

FIG. 7. Model cell's response to different external current levels. At t = 500 ms, a 1-s-long pulse of current is applied. i_{ext} level for each condition is indicated in nanoamperes on the *top right corner* of each panel.

DISCUSSION

The model LP neuron behaves in a manner gratifyingly similar to that of the real LP neuron. The model neuron fires tonically at rest, increases its rate appropriately when depolarized, and stops firing when hyperpolarized. When the model LP is strongly hyperpolarized, it also displays a "sag" in the voltage response that mimics what is seen in the biological LP neuron. Additionally, the steady-state *I-V* curves of the model and the biological LP neurons resemble each other closely, although there is a slight inflection point in the *I-V* curve of the model that does not occur in the biological neuron.

The model was constructed from six voltage-dependent conductances, a leakage conductance, a Ca^{2+} buffering system, and a capacitance. The model differs from the measurements on the biological neuron in two regards: the model generates overshooting action potentials, and its capacitance is lower than the measured value (Golowasch and Marder 1992a). Indeed the model we built is more properly thought of as a model of the cell at the action-potential initiation zone. As such, the model, with its lowered capacitance, reflects a smaller area of the cell's total surface. It should be stressed that the capacitance and the parameters that characterize i_{Na} were the only "free" parameters in the model that we manipulated to make the model behave. It is interesting that the model is sensitive to the parameters of i_{Na}, and that the parameters we settled on, with the capacitance value of the final model, produce robust behavior that conforms to physiological recordings under a variety of perturbations, described in this and the following paper (Golowasch et al. 1992).

We know that the LP neuron must have more than a single compartment (Golowasch and Marder 1992a). Therefore this isopotential model certainly represents an oversimplification of the LP neuron. However, the relatively faithful rendering of the real cell's activity and the relative simplicity of this model allow us to explore the role of each of the conductances in the excitability of the neuron. More sophisticated versions, including geometrical complexities and nonhomogeneous distributions of currents over the dendritic tree (Traub et al. 1991), may be necessary to obtain more accurate representations of cellular activity. Indeed, preliminary results with a two-compartment model in which the soma and proximal neurite are devoid of i_{Na} show improved robustness and attenuated action potentials as well as a more realistic membrane capacitance (F. Buchholtz, unpublished observations).

A multicompartment model, like the one reported by Traub et al. (1991), may become essential in the future when more detailed studies of current density distributions and of receptor and synapse distributions become available. To some extent we know already that at least γ-aminobutyric acid (GABA) receptors (Golowasch 1990), proctolin receptors (Golowasch and Marder 1992b), Na^+ currents (Miller 1975; Raper 1979), and Ca^{2+} currents (Graubard

and Ross 1985; Ross and Graubard 1989) are unevenly distributed over the cell's surface, but no details on the distributions are known.

The simplicity of our equations [the forward and backward rate equations of the Hodgkin-Huxley model are reduced to sigmoidal functions of voltage (*Eq. 2*)] is a mixed blessing. On the one hand, it simplifies the calculations and reduces the number of parameters enormously. On the other hand, it lacks the detailed description other models contain (DiFrancesco and Noble 1985; Hodgkin and Huxley 1952; Traub et al. 1991; Yamada et al. 1989). However, the equations we have used are mathematically equivalent to the Hodgkin-Huxley equations, and the enormous variability one observes in biological systems makes a more detailed description of the individual currents of unclear significance.

The parameters of the Na^+ current we use differ from those in squid axon (Hodgkin and Huxley 1952), crab walking leg axon (Connor et al. 1977), and bullfrog sympathetic ganglion (Yamada et al. 1989). For example, V_{am} is $\sim$25 mV more negative, and s_{ah} and s_{bh} are $\sim$10 mV more negative here than in either the squid axon or the walking leg axons (Connor et al. 1977; Hodgkin and Huxley 1952) (see Table 1). In other simulations, we tried the parameters for i_{Na} from the walking axon of two different species of crab (Connor et al. 1977) in conjunction with the other currents we have recorded in the LP cell (Golowasch and Marder 1992a,b) but were not able to generate a pattern of activity consistent with the LP cell's activity.

The properties of the Ca^{2+} buffering system are likely to be oversimplified (*Eq. 12*). The intracellular [Ca] dynamics of the model has a time constant of less than one-half a second (k_{Ca} in Table 1), whereas the estimated time constant of Ca^{2+} removal in the LP cell is of the order of seconds (Golowasch 1990), similar to what has been measured in other cell types (Chad and Eckert 1984; Hernández-Cruz et al. 1990). However, both our measurements of the time constant of removal of Ca^{2+} from the LP cell (Golowasch 1990) as well as the results from Ca^{2+} imaging (Chad and Eckert 1984; Hernández-Cruz et al. 1990) correspond to averages of [Ca] throughout the entire volume of the cell and, therefore, do not necessarily provide an accurate definition of appropriate kinetic parameters for this process. This indicates that our simplified version of the intracellular [Ca] dynamics may not be correct, and that a more complex model (cf. Chad and Eckert 1984; Hernández-Cruz et al. 1990; Kramer and Zucker 1985; Zucker 1989) may be required. However, see Traub et al. (1991).

It is interesting to compare the model LP neuron with other experimentally based, well-characterized cellular models. The B cells of the bullfrog sympathetic ganglion are similar to the LP cell. Both cell types express variations of a delayed rectifier, an A-current, a Ca^{2+} current, a Ca^{2+}-activated K^+ current, and a fast Na^+ current. Nevertheless, there are some important differences; the LP cell additionally expresses an inward rectifier similar to i_f of the Purkinje cell (DiFrancesco and Noble 1985), which the B cells lack. The bullfrog B cells express two additional currents that the LP cell lacks: the noninactivating M-current and the voltage-independent, Ca^{2+}-activated current i_{AHP} (Yamada et al. 1989). Both of these currents play a role that resembles that described for i_{proc} in the following paper: both are small, and both can activate around V_{rest} and close to the action-potential threshold, thus playing a critical role in determining cellular excitability in spite of their low amplitude (Yamada et al. 1989).

Another recently published model is that of hippocampal CA3 and CA1 neurons (Traub et al. 1991). This model shares with our LP cell model a number of conductances, (i_{Na}, i_{Ca}, $i_{o(Ca)}$, and i_d). But in the model of Traub et al. (1991), as in the case of that of Yamada et al. (1989), $i_{K(AHP)}$ seems to play a subtle but important role in regulating the cell's excitability, in a way that resembles the subtle effects of i_{proc} described in the accompanying paper (Golowasch et al. 1992).

In conclusion, we have generated a set of equations that describe the independently measured ionic conductances described previously (Golowasch and Marder 1992a,b). The integration, in a single-compartment model cell of the currents they describe, reproduces well the activity pattern of the LP cell in spite of the assumptions we are forced to make given the experimental restrictions this cell imposes. In the following paper (Golowasch et al. 1992) we test the model further by comparing the effects of modifications of individual currents with those of pharmacological manipulations of the biological cell. Additionally, we add another current to the model, the inward current activated by proctolin (i_{proc}), a modulator of LP activity (Golowasch and Marder 1992b), and compare the activity of the real and the model cell in response to proctolin applications. Furthermore, we study the development of each individual current during the free running activity of the model in the presence and in the absence of proctolin, showing that i_{proc} induces changes in the contributions of other independent currents to the activity pattern of the cell.

We thank Drs. L. F. Abbott and John Lisman for valuable comments. This paper benefited greatly from the comments of the *Journal of Neurophysiology* reviewers.

This work was supported by the National Institute of Mental Health Grant MH-46742 and by a fellowship from the Deutsche Forschungsgemeinschaft to F. Buchholtz.

J. Golowasch submitted part of this work in partial fulfillment of the requirements for the PhD in Biophysics at Brandeis University.

Present address of J. Golowasch, Laboratoire de Neurobiologie, Ecole Normale Supérieure, 46 rue d'Ulm, 75005 Paris, France.

Address for reprint requests: E. Marder, Dept. of Biology, Brandeis University, Waltham, MA 02254-9110.

Received 31 May 1991; accepted in final form 4 September 1991.

REFERENCES

BARRETT, J. N., MAGLEBY, K. L., AND PALLOTTA, B. S. Properties of single Ca^{2+}-activated K^+ channels in cultured rat muscle. *J. Physiol. Lond.* 331: 211–230, 1982.

CANAVIER, C. C., CLARK, J. W., AND BYRNE, J. H. Routes to chaos in a model of a bursting neuron. *Biophys. J.* 57: 1245–1251, 1990.

CHAD, J. E. AND ECKERT, R. Calcium domains associated with individual channels can account for anomalous voltage relations of Ca-dependent responses. *Biophys. J.* 45: 993–999, 1984.

CONNOR, J. A., WALTER, D., AND MCKOWN, R. Neural repetitive firing. Modifications of the Hodgkin-Huxley axon suggested by experimental results from crustacean axons. *Biophys. J.* 18: 81–102, 1977.

DIFRANCESCO, D. AND NOBLE, D. A model of cardiac electrical activity incorporating ionic pumps and concentration changes. *Philos. Trans. R. Soc. Lond. Biol. Sci.* 307: 353–398, 1985.

EPSTEIN, I. R. AND MARDER, E. Multiple modes of a conditional neural oscillator. *Biol. Cybern.* 63: 25–34, 1990.

GOLOWASCH, J. *Characterization of a Stomatogastric Ganglion Neuron. A Biophysical and a Mathematical Description* (PhD dissertation). Waltham, MA: Brandeis Univ., 1990.

GOLOWASCH, J., BUCHHOLTZ, F., EPSTEIN, I. R., AND MARDER, E. Contribution of individual ionic currents to activity of a model stomatogastric ganglion neuron. *J. Neurophysiol.* 67: 341–349, 1992.

GOLOWASCH, J. AND MARDER, E. Ionic currents of the lateral pyloric neuron of the stomatogastric ganglion of the crab. *J. Neurophysiol.* 67: 318–331, 1992a.

GOLOWASCH, J. AND MARDER, E. Proctolin activates an inward current whose voltage dependence is modified by extracellular Ca^{2+}. *J. Neurosci.* In press, 1992b.

GRAUBARD, K. AND ROSS, W. N. Regional distribution of calcium influx into bursting neurons detected with Arsenazo III. *Proc. Natl. Acad. Sci. USA* 82: 5565–5569, 1985.

HERNÁNDEZ-CRUZ, A., SALA, F., AND ADAMS, P. R. Subcellular calcium transients visualized by confocal microscopy in a voltage-clamped vertebrate neuron. *Science Wash. DC* 247: 858–862, 1990.

HODGKIN, A. L. AND HUXLEY, A. F. A quantitative description of membrane current and its application to conduction and excitation in nerve. *J. Physiol. Lond.* 117: 500–544, 1952.

HOOPER, S. L. AND MARDER, E. Modulation of the lobster pyloric rhythm by the peptide proctolin. *J. Neurosci.* 7: 2097–2112, 1987.

KRAMER, R. H. AND ZUCKER, R. Calcium-dependent inward current in *Aplysia* bursting pacemaker neurons. *J. Physiol. Lond.* 362: 107–130, 1985.

MILLER, J. Neuropile recordings in the lobster stomatogastric ganglion. *Soc. Neurosci. Abstr.* 1: 579, 1975.

MOCZYDLOWSKI, E. AND LATORRE, R. Gating kinetics of Ca^{2+}-activated K^+ channels from rat muscle incorporated into planar lipid bilayers. *J. Gen. Physiol.* 82: 511–542, 1983.

PLANT, R. E. AND KIM, M. Mathematical description of a bursting pacemaker neuron by a modification of the Hodgkin-Huxley equations. *Biophys. J.* 16: 227–244, 1976.

PRESS, W. H. *Numerical Recipes: the Art of Scientific Computing.* Cambridge, UK: Cambridge Univ. Press, 1986.

RAPER, J. A. Nonimpulse-mediated synaptic transmission during the generation of a cyclic motor program. *Science Wash. DC* 205: 304–306, 1979.

ROSE, R. M. AND HINDMARSH, J. L. The assembly of currents in a thalamic neuron. I. The three-dimensional model. *Proc. R. Soc. Lond. B Biol. Sci.* 237: 267–288, 1989a.

ROSE, R. M. AND HINDMARSH, J. L. The assembly of currents in a thalamic neuron. II. The stability and state diagrams. *Proc. R. Soc. Lond. B Biol. Sci.* 237: 289–312, 1989b.

ROSE, R. M. AND HINDMARSH, J. L. The assembly of currents in a thalamic neuron. III. The seven-dimensional model. *Proc. R. Soc. Lond. B Biol. Sci.* 237: 313–334, 1989c.

ROSS, W. N. AND GRAUBARD, K. Spatially and temporally resolved calcium concentration changes in oscillating neurons of crab stomatogastric ganglion. *Proc. Natl. Acad. Sci. USA* 86: 1679–1683, 1989.

TRAUB, R. D., WONG, R. K. S., MILES, R., AND MICHELSON, H. A model of a CA3 hippocampal pyramidal neuron incorporating voltage-clamp data on intrinsic conductances. *J. Neurophysiol.* 66: 635–650, 1991.

YAMADA, W. M., KOCH, C., AND ADAMS, P. Multiple channels and calcium dynamics. In: *Methods in Neuronal Modeling. From Synapses to Networks,* edited by C. Koch and I. Segev. Cambridge, MA: MIT Press, 1989, p. 97–134.

ZUCKER, R. S. Models of calcium regulation in neurons. In: *Neural Models of Plasticity. Experimental and Theoretical Approaches,* edited by J. H. Byrne and W. O. Berry. San Diego, CA: Academic, 1989, p. 403–422.